In situ Carbon Modification of g-C_3N_4 from Urea Co-crystal with Enhanced Photocatalytic Activity Towards Degradation of Organic Dyes Under Visible Light

ZHAO Weifeng[1*], HAO Ning[1], ZHANG Gai[1], MA Aijie[1], CHEN Weixing[1*], ZHOU Hongwei[1], YANG Dong[2], XU Ben Bin[3] and KONG Jie[2*]

1. School of Materials and Chemical Engineering, Xi'an Technological University, Xi'an 710021, P. R. China;
2. Department of Applied Chemistry, School of Science, Northwestern Polytechnical University, Xi'an 710072, P. R. China;
3. Department of Mechanical and Construction Engineering, Faculty of Engineering and Environment, Northumbria University, Newcastle upon Tyne, NE1 8ST, UK

Abstract An *in situ* strategy was introduced for synthesizing carbon modified graphitic carbon nitride(g-C_3N_4) by using urea/4-aminobenzoic acid(PABA) co-crystal(PABA@Urea) as precursor materials. *Via* co-calcination of the PABA co-former and the urea in PABA@Urea co-crystals, C guest species were generated and compounded into g-C_3N_4 matrix *in situ* by replacing the lattice N of the carbon nitride and forming carbon dots onto its layer surface. The carbon modification dramatically enhanced visible-light harvesting and charge carrier separation. Therefore, visible light photo-catalytic oxidation of methylene blue(MB) pollution in water over the carbon modified g-C_3N_4 (C/g-C_3N_4) was notably improved. Up to 99% of methylene blue(MB) was eliminated within 60 min by the optimal sample prepared from the PABA@Urea co-crystal with a PABA content of 0.1%(mass ratio), faster than the degradation rate over bare g-C_3N_4. The present study demonstrates a new way to boost up the photocatalysis performance of g-C_3N_4, which holds great potential concerning the degradation of organic dyes from water.

Keywords Graphitic carbon nitride; Carbon composite; Photocatalysis; Photodegradation

1 Introduction

As a non-metallic conjugated polymer, g-C_3N_4 has been of research focus in recent years for its high thermal and physico-chemical stability, attractive semi-conductivity, facile synthesis, low cost and earth-abundant resources[1—3]. The optical band gap of *ca.* 2.7 eV gives g-C_3N_4 a wide and strong absorption of solar spectrum. However, the fast recombination of photo-induced electrons and holes limiting electronic conduction, and insufficient light absorption beyond 460 nm greatly hinder the light-driven catalytic performance of g-C_3N_4. Various approaches were thus developed to address this issue, such as heteroatom doping[4—6], constructing heterostructure[7—9], edge-functionalization[10], morphology control[11—13], and combining g-C_3N_4 with carbonaceous materials[14—16]. During the past years, several kinds of organics have been reported to construct C doped g-C_3N_4. For example, Li and coworkers[17] prepared carbon bridged g-C_3N_4 with chitosan as carbon precursor, achieving a H_2 generation rate 7 times higher that of bulk g-C_3N_4. Panneri *et al.*[18] utilized spray drying to granulate g-C_3N_4 nanosheets into microspheres with high surface area that was superior in removing tetracycline antibiotic by adsorption and photocatalytic degradation. Although the previous researches have demonstrated a strong relationship between the photocatalytic properties and the delocalized π bonds between the heptazine units of g-C_3N_4, the self-doping strategy is still a challenge for the decorating of g-C_3N_4 because it contains no mental and oxygen elements.

Molecular cooperative assembly is a process widely used in crystal engineering, by which the molecules can be spontaneously arranged *via* non-covalent interactions to form stable aggregates[19]. Although g-C_3N_4 with different nano-structured architectures has been achieved from supramolecular assembled aggregates of melamine precursor and triazine derivatives (*e.g.*, cyanuric acid)[20—22], to the best of our knowledge, there are few researches concerning the modification of g-C_3N_4 using urea based assembled complex. Copyrolysis is an effective method to synthesize carbon-rich hybrid materials from organic precursors[23—25]. Herein, a new strategy was established for producing carbon modified g-C_3N_4(C/g-C_3N_4) through

*Corresponding authors. Email: zhaoweifeng@xatu.edu.cn; chenwx@xatu.edu.cn; kongjie@nwpu.edu.cn
Received March 25, 2020; accepted May 20, 2020.
Supported by the National Natural Science Foundation of China(Nos.61604120, 51603164), the Natural Science Foundation of Shaanxi Province, China(No.2019JM-527), the Natural Science Basic Research Plan in Shaanxi Province, China (No.2018JC-008), the Key Research and Development Plan for Industry Innovation Chain(Cluster) of Shaanxi Province, China (No.2018ZDCXL-GY-09-07).

pyrolysis urea/4-aminobenzoic acid(PABA) co-crystals (PABA@Urea). The urea acted as precursors for g-C_3N_4 and the co-formers PABA was the source for C guest species (Scheme 1). The enhancement of g-C_3N_4 photocatalytic activity was evidenced by decomposing methylene blue(MB) dyes from water under visible light irradiation.

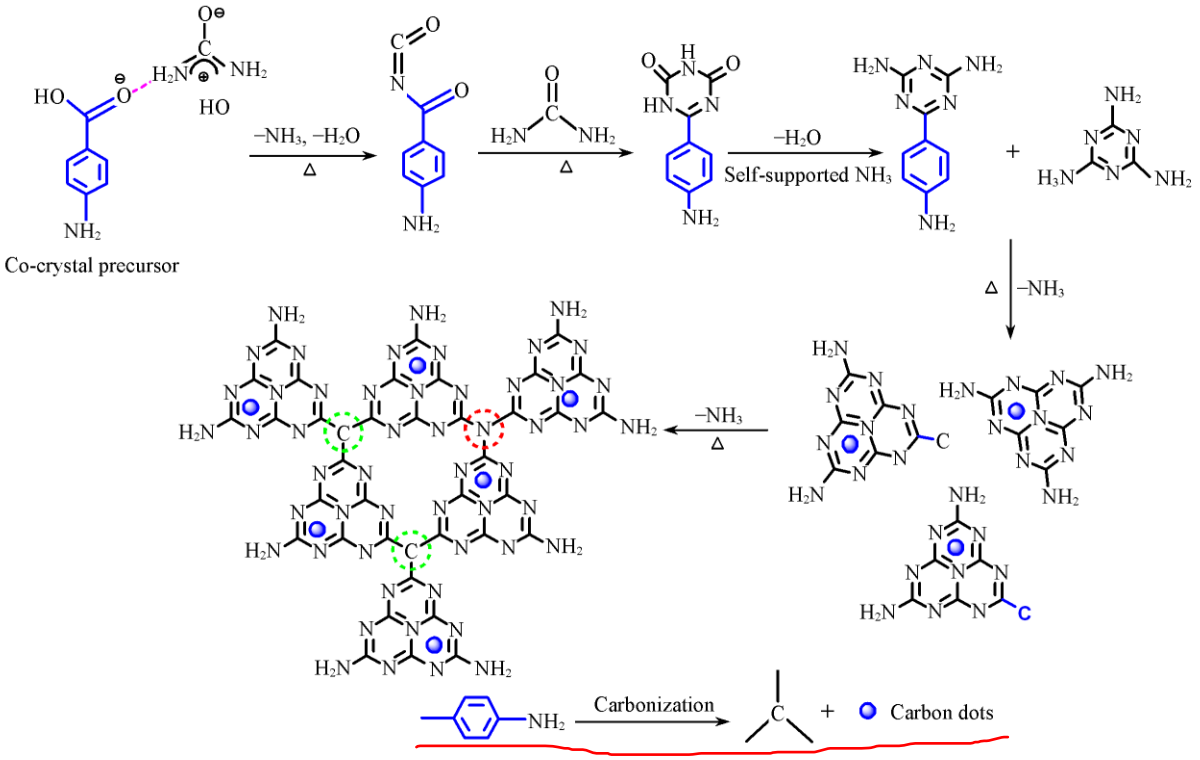

Scheme 1 Schematically illustration for producing carbon bridged g-C_3N_4 decorated with carbon dots from PABA@Urea co-crystal precursor

The green and red circles indicate the bridging atoms of C and N, respectively.

2 Expetimental

2.1 Synthesis of g-C_3N_4 Photocatalysts

Urea(AR), 4-aminobenzoic acid(PABA, AR) and methylene blue(MB) supplied by Shanghai Civi Company(China) were used as received. Bulk g-C_3N_4 was fabricated *via* polymerizing urea at 550 ℃ in ambient atmosphere for 3 h according to the literature[26]. To synthesize C/g-C_3N_4, PABA(0.02, 0.04, 0.08 and 0.16 g) and urea(40.0 g) were dissolved into ethanol (250 mL), and then the ethanol solvent was evaporated gradually. The obtained white solid PABA@Urea co-crystals with PABA mass contents of 0.05%, 0.1%, 0.2% and 0.4% were collected and dried in an oven. Subsequently, the PABA@Urea co-crystals were calcined in a muffle furnace at 550 ℃ in ambient atmosphere for 3 h, the same as that for the preparation of bulk g-C_3N_4, giving the final products labeled as C/g-C_3N_4 (PABA: 0.05%), C/g-C_3N_4(PABA: 0.1%), C/g-C_3N_4(PABA: 0.2%) and C/g-C_3N_4(PABA: 0.4%).

2.2 Characterization

Fourier transform infrared(FTIR) spectra were recorded on a Vertex-70 FTIR spectrometer(Bruker, Germany). The sample was mixed with air dried potassium bromide powder and compressed into a thin pellet for the FTIR examination. X-Ray diffraction(XRD) patterns were obtained on an XRD-6000 diffractometer(Shimadzu, Japan) with the angle of 2θ ranging from 5° to 60°. The scanning speed was set to 2°/min with an step size of 0.02°. UV-Vis diffuse reflection spectra(DRS) were collected using a Agilent Cary 5000 UV-Vis spectrophotometer. Optical absorbance of MB solution was recorded on a UV spectrophotometer(Shimadzu UV2550, Japan) at room temperature. BET surface area was measured using a NOVA 3200e specific surface area tester(Conta, USA). Prior to the BET measurement, all the samples were degassed at 300 ℃ for 3 h. Morphologic images was characterized using a VEGA2 scanning electron microscope(TESCON, Czech) and a transmission electron microscope(FEI Talos-F200X). X-Ray photoelectron spectroscopy(XPS) was conducted on an Axis-Ultra spectrometer(Kratos, UK) with an Al $K\alpha$ radiation source. Photoluminescence(PL) was taken on a fluorescence spectrophotometer(LS55, American) from PE Company with the excitation wavelength fixed at 325 nm. Electrochemical impedance spectra(EIS) were measured using an electrochemical workstation(CHI650E, Chenhua, China), with platinum foil as the counter electrode and an Ag/AgCl(in saturated KCl) electrode as the reference electrode. Na_2SO_4 aqueous solution (0.5 mol/L) and nickel foam were employed as electrolyte and working electrode, respectively.

2.3 Photocatalytic Activity Evaluation

Photocatalyst samples(30 mg) were sonicated in 50 mL of MB aqueous solutions for 10 min to make a homogeneous dispersion. The mixture was then stirred in darkness till

achieving an equilibrium between adsorption and desorption. Subsequently, photocatalytic reaction was triggered under visible light(λ>420 nm) emitted through a UV-cutoff filter from a 300 W xenon arc lamp. At a given irradiation interval, a small aliquot(2.5 mL) of the sample was taken and recovered. The MB content in the recovered supernatant solution was monitored by means of UV-Vis spectroscopy *via* examining the optical absorption values at 664 nm with a previously established calibration curve.

3 Results and Discussion

Solution crystallization is an excellent approach to obtain co-crystals. Both urea and PABA are soluble in ethanol, so supramolecular co-crystals can be obtained by molecular assembly between them when the ethanol solvent was removed gradually(Fig.S1, see the Electronic Supplementary Material of this paper). PABA has a low thermal stability and began to decompose at *ca.* 170 ℃ and was carbonized at the temperature near 400 ℃(Fig.S2, see the Electronic Supplementary Material of this paper). During the co-calcinations process, condensation and polymerization reactions starting from the urea monomers occurred, accompanying with the carbonization of the PABA, giving carbon bridged g-C_3N_4 decorated with carbon dots (Scheme 1).

Fig.1 displays XRD patterns of pure g-C_3N_4 and various C/g-C_3N_4 samples prepared from the PABA@Urea precursors containing different amount of PABA co-formers. As can be seen from Fig.1, in accordance with the XRD characteristics of pure g-C_3N_4, all the C/g-C_3N_4 samples are characterized by an obvious diffraction peak at 2θ=27.8 °, and a minor diffraction at around 2θ=13.0 °. The peak at 2θ=27.8 °is assigned to the (002) diffraction of g-C_3N_4 due to the graphitic stacking feature. Whereas, the minor one at 2θ=13.0 °is correspond to the (100) diffraction of g-C_3N_4 sheets resulted from their repeated in-plane tri-*s*-triazine unit. The similarity between the XRD patterns of pure g-C_3N_4 and C/g-C_3N_4 samples suggests that g-C_3N_4 matrix has been formed from the PABA@Urea precursors[27,28]. Nevertheless, the intensity of (002) diffraction peak decrease, gradually with increasing PABA content in PABA@Urea. This might be due to that the PABA co-formers prevent the polymerization of urea and hinder the g-C_3N_4 layers stacking, leading to lattice distortion in g-C_3N_4 matrix[29].

SEM and TEM were conducted to further verify the structural features of C/g-C_3N_4. As shown in Fig.2(A) and (B), both pristine g-C_3N_4 and the C/g-C_3N_4 samples displayed an aggregated morphology consisting of irregular shaped layers, suggesting that the addition of PABA and followed carbonization do not destroy the layered structure feature of g-C_3N_4, well agrees with the XRD results displayed in Fig.1. However, different from pure g-C_3N_4, where the sheets are relative large and packed densely, the C/g-C_3N_4 samples displayed a relatively loose structure comprising smaller sheets and pores. The lamellar skeleton of C/g-C_3N_4 was also confirmed by TEM analysis. As demonstrated in Fig.2(C), a wrinkled paper-like structure with in-plane holes(indicated by the white arrows) was observed for the C/g-C_3N_4 catalysts. This will give more active sites for photocatalytic reactions. Moreover, as shown in Fig.2(D)—(F), similar to the morphology of carbon dots/g-C_3N_4 composite reported by others[30], high magnification TEM images of the C/g-C_3N_4 samples clearly demonstrate the presence of carbon dots(indicated with red circles) onto the g-C_3N_4 sheet surface, which will enhance the photocatalytic efficiency, too.

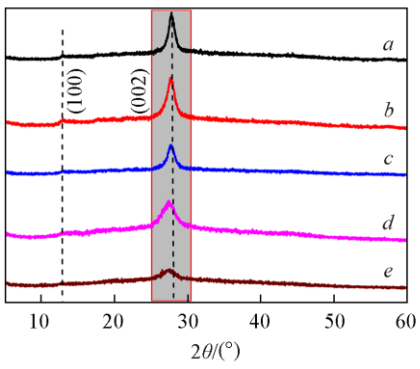

Fig.1 XRD patterns of pure g-C_3N_4 and the C/g-C_3N_4 photocatalysts prepared from PABA@Urea with different PABA mass contents

a. g-C_3N_4; *b*—*e*: C/g-C_3N_4 with mass ratios of 0.05%, 0.1%, 0.2%, 0.4% of PABA.

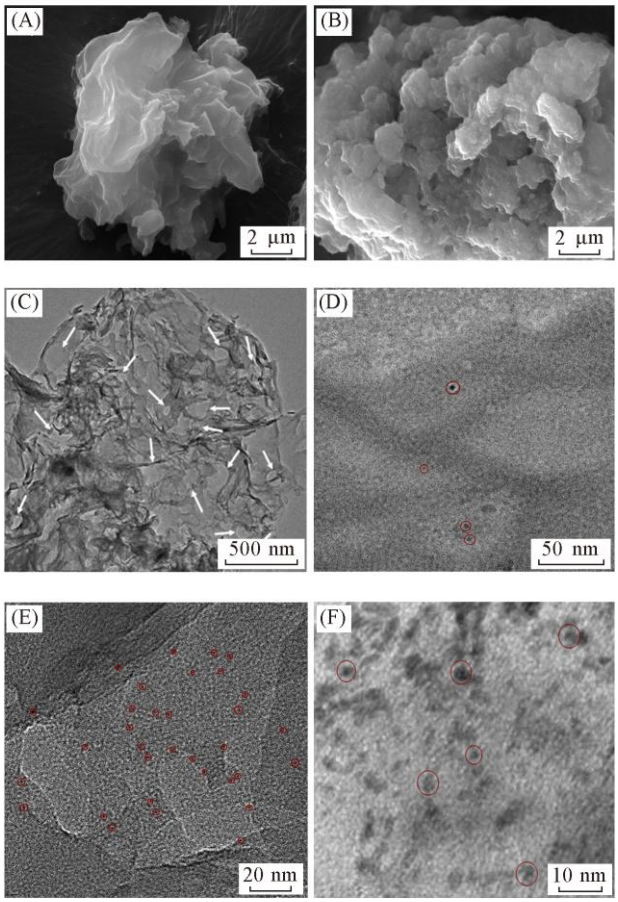

Fig.2 SEM images of g-C_3N_4(A) and C/g-C_3N_4(B), and TEM images of C/g-C_3N_4 at a relatively low(C) and higher magnifications(D—F)

The white arrows and red circles indicate the pores and C dots on the sheet surface, respectively.

N_2 adsorption-desorption measurement also confirms the mesoporous textural structure of C/-g-C_3N_4 hybrid catalysts (Fig.3). For example, it was measured that the C/g-C_3N_4(PABA 0.1%) possess a surface area of 88.707 m^2/g and total pore volume of 0.2911 cm^3/g, much higher than those of pristine g-C_3N_4(46.736 m^2/g and 0.1644 cm^3/g).

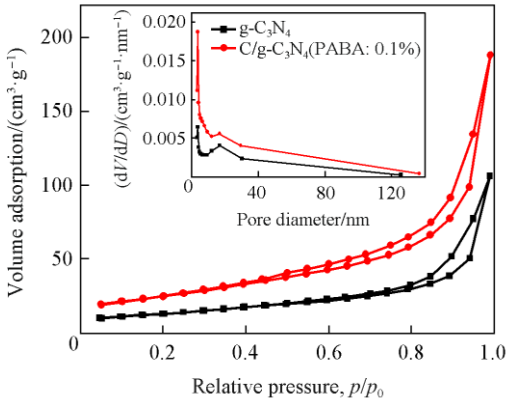

Fig.3 N_2 adsorption-desorption isotheres and pore size distribution plots(inset) of g-C_3N_4 and C/g-C_3N_4(PABA: 0.1%)

FTIR and XPS were carried out to illustrate the chemical compositions and atoms state in C/g-C_3N_4. XPS survey spectra reveal both g-C_3N_4 and C/g-C_3N_4 composite mainly contain C and N elements deriving from g-C_3N_4[Fig.4(A)]. Whereas, the tiny amount of O may be due to the H_2O and C—O—H groups absorbed on the sample surface[31,32]. From the high resolution C_{1s} spectrum[Fig.4(B)], three bands at 284.4, 285.7 and 287.8 eV were detected, ascribed to the sp^2-hybridized C involved in C—C/C═C bond[30,33,34], C—NH_2 species[35] and N═C—N[36,37], respectively. Interestingly, the ratio of C—C and N═C—N peak area(C—C/N═C—N) is calculated to be 1.584 for C/g-C_3N_4, higher than the value for pristine g-C_3N_4 (1.562), demonstrating that additional carbon specifies have been compounded into the g-C_3N_4 matrix by the doping treatment. The N_{1s} spectrum also confirms the success of C doping in g-C_3N_4. As illustrated in Fig.4(C), three characteristic peaks assigned to N in C═N—C, N—C_3, and C—N—H are observed at 398.0, 399.5 and 400.5eV, respectively[38—40]. The calculated area ratio of sp^3 nitrogen to sp^2 nitrogen (N—C_3/C═N—C) was decreased from 0.333 for g-C_3N_4 to 0.318 for C/g-C_3N_4, again reflecting the substitution of bridging N by C atoms in g-C_3N_4 skeleton because of C self-doping[17,41]. In Fig.5, characteristic absorptions related to CN heterocycles (1240—1640 cm^{-1}) and *s*-triazine units(810 cm^{-1}) from g-C_3N_4 are distinctly observed in FTIR spectra of C/g-C_3N_4[42,43], which indicates that the overall skeleton of g-C_3N_4 keeps intact after the *in-situ* C modification. This is in accordance with the XRD results. Additionally, it can be found that the intensity of triazine unit absorption peak at 810 cm^{-1} decreases gradually with an increase of the PABA content in the co-crystal precursor from 0.05% to 0.4%(mass ratio). This can be well interpreted by the partial replacement of bridging N with the self doped C atoms in the g-C_3N_4 skeleton, which will decrease the absorption ability of the triazine units.

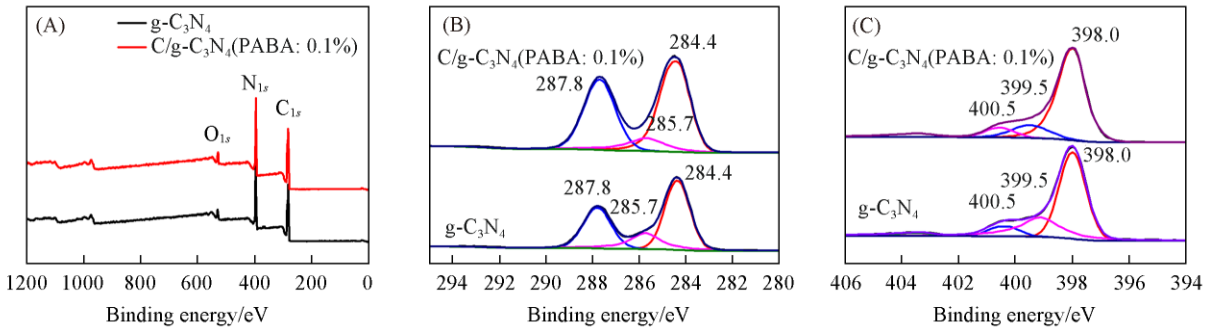

Fig.4 XPS spectra of g-C_3N_4 and C/g-C_3N_4(PABA: 0.1%)

(A) Survey spectra; (B) C_{1s};(C) N_{1s}.

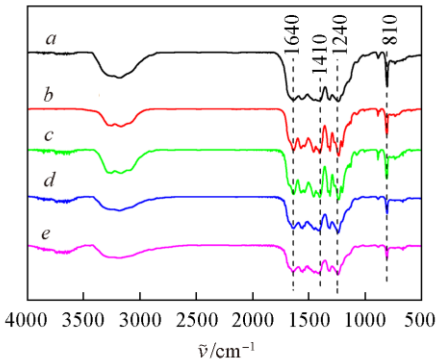

Fig.5 FTIR spectra of the photocatalyst samples prepared from PABA@Urea with varying PABA loading amount

a. g-C_3N_4; *b*. C/g-C_3N_4(PABA: 0.05%); *c*. C/g-C_3N_4(PABA: 0.1%); *d*. C/g-C_3N_4(PABA: 0.2%); *e*. C/g-C_3N_4(PABA: 0.4%).

UV-Vis DRS measurement reveals a dramatic red shift of intrinsic absorption edges of the C/g-C_3N_4 samples with increasing carbon doping content(Fig.6). Calculated from the Kubelka-Munk function, the derived band energies corresponding to bulk g-C_3N_4, C/g-C_3N_4(PABA: 0.05%), C/g-C_3N_4 (PABA: 0.1%), C/g-C_3N_4(PABA: 0.2%) and C/g-C_3N_4(PABA: 0.4%) were 2.75, 2.67, 2.56, 2.06 and 1.77 eV, respectively. Moreover, the C/g-C_3N_4 samples have a much stronger tail absorption to light from 450 nm to 800 nm, owing to the midgap state caused by the distortions or defects in the C/g-C_3N_4, in addition to an enhanced absorption intensity from the UV to blue region. In fact, the doping-induced distortions/defects play an important role in photo-electrochemical activities of carbon based materials, including g-C_3N_4[44]. The absorption spectra suggest that the presence of doped carbon and defects in g-C_3N_4 could effectively promote the light

harvesting capability, which is favoured for the improvement of photocatalytic performance.

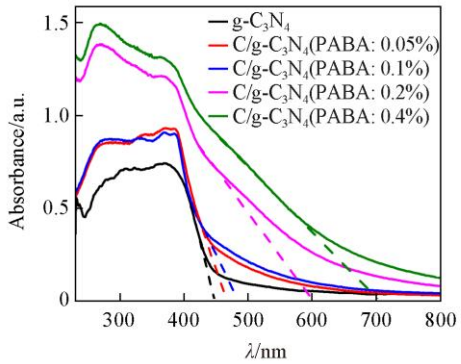

Fig.6 UV-Vis DRS of g-C_3N_4 and C/g-C_3N_4 prepared from PABA@Urea

The photocatalytic activities of pristine g-C_3N_4 and the C/g-C_3N_4 photocatalysts were evaluated by elimination of MB dyes in water under visible light. Prior to light illumination**,** the mixtures of photocatalysts and MB dyes in water were stirred in darkness for 120 min to obtain the absorption-desorption equilibrium between dyes and photocatalysts. As shown in Fig.7(A), the MB concentration tends to keep constant after a slightly decrease during the dark stirring process, suggesting the establishment of adsorption-desorption equilibrium between MB and the photocatalyst samples. Subsequently, photo-degradation of MB over g-C_3N_4, and over the photocatalysts of C/g-C_3N_4 photocatalysts was carried out under visible light irradiation. It is found that all the photocatalysts are capable of degrading the

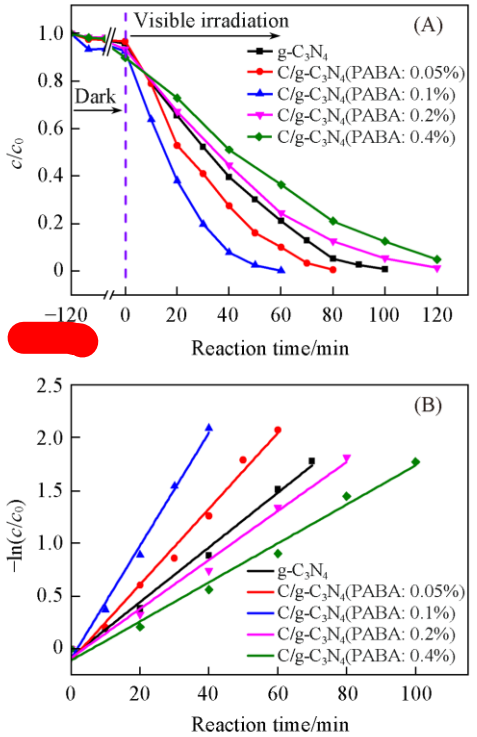

Fig.7 Photocatalytic MB degradation performance of g-C_3N_4 and C/g-C_3N_4 samples under visible light illumination

(A) Variation of MB concentration *versus* reaction time; (B) pseudo-first-order kinetics curves of MB elimination over samples.

MB pollutants, resulting in obvious decrease of the MB concentrations. However, compared with pristine g-C_3N_4, the carbon modified C/g-C_3N_4 catalysts derived from PABA@Urea co-crystals with 0.05% and 0.1%(mass content) of PABA, exhibit a notable improved degradation efficiency. The C/g-C_3N_4(PABA: 0.1%) can degrade more than 99% of MB dyes within 60 min, much more efficient than the degradation rate over bare g-C_3N_4, of which 80% MB was decomposed during the same period. Meanwhile, it is also found that the photocatalytic activity tends to decrease with a further increasing of PABA. This may be due to that the excessive C can also act as a recombinant centre, and might prevent the incident light absorption of g-C_3N_4 owning to the shadowing effect[45], therefore reducing the photo-reactivity of the photo-catalysts. The degradation of MB could well fit pseudo-first-order kinetics that can be described by a Langmuir-Hinshelwood model with the following equation: $\ln(c/c_0)=-k_a t$, where k_a is the apparent pseudo-first-order rate constant and t is the reaction time. By plotting $-\ln(c/c_0)$ *versus* reaction time(t), pseudo-first-order kinetics curves of the MB elimination over the catalysts were obtained, which shows a perfect linear relationship, as shown in Fig.7(B). The pseudo-first-order rate constant k_a is 0.054 min^{-1} for C/g-C_3N_4(PABA:0.1%) and is 0.026 for prinstine g-C_3N_4, clearly demonstrating an enhancement of photocatalytic activity by the carbon doping treatment. In addition, for practical applications, catalyst materials having long-term stability are always required. Recycling experiments were further carried out to evaluate the reusability of the C/g-C_3N_4 photocatalysts. As shown in Fig.8, the MB solution can be almost completely degraded within 60—70 min for each of the four circles. No obvious decrease in degradation rate can be observed over the four times consecutive recycling utilization, indicating the photocatalyst is of good stability under long-term irradiation.

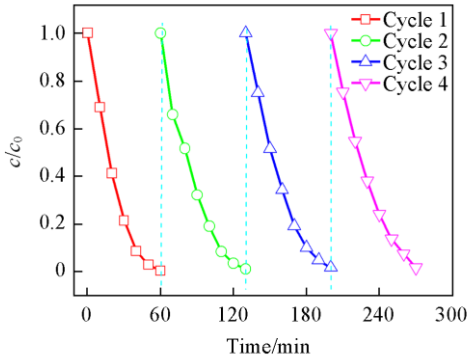

Fig.8 Photocatalytic MB elimination over C/g-C_3N_4 (PABA:0.1%) with four times of cycling uses

To deeply understand the reasons for the photocatalytic MB degradation enhancement, PL and EIS analyses were performed to probe the charge transfer, separation and recombination properties. As depicted in Fig.9(A), bulk g-C_3N_4 displayed a PL pattern with strong emission centered at 460 nm, corresponding to a highly charge carrier recombination[43,46]. In contrast to g-C_3N_4, the fluorescence of C/g-C_3N_4 was quenched significantly, suggesting reduced charge recombination and accelerated charge separation in the carbon doped catalyst[39,42].

In addition, both the bridging C atoms and the introduced carbon dots could act as transporters for electrons and make the π system of g-C_3N_4 extend, resulting in an increase in electrical conductivity. As shown in Fig.9(B), the EIS Nyquist plots show that C/g-C_3N_4 displays a smaller semicircle diameter compared with pristine g-C_3N_4, indicative of lower charge transfer resistance in the carbon doped samples. These results can be well interpreted by the carbon doping modifications. The HOMO and LUMO positions of g-C_3N_4 are located at about +1.4 and −1.3 eV[*vs.* normal hydrogen electrode(NHE), pH=7], respectively[47]. Its CB energy level is negative sufficiently for photoreduction reactions. Whereas, for the carbon dots, its HOMO level is in the middle of bandgap of g-C_3N_4, while the LUMO is more negative than the CB of g-C_3N_4[48]. Therefore, the hybrid C/g-C_3N_4 can form a type-II heterojunction as illustrated in Scheme 2. In the type-II heterojunction, the photo-induced

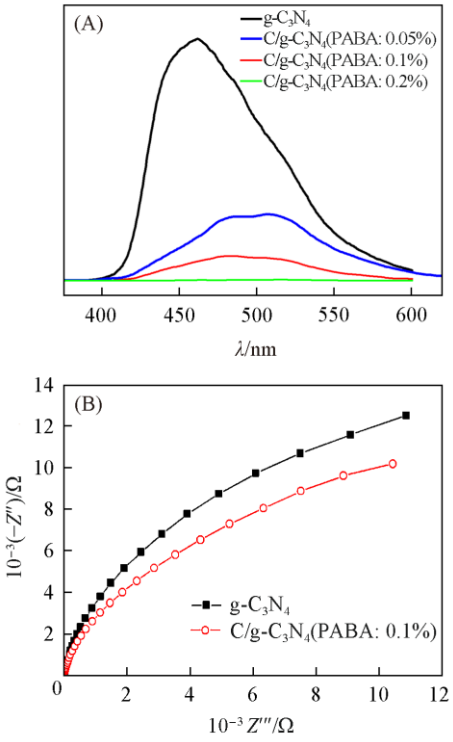

Fig.9 PL spectra(A) and EIS Nyquist plots(B) of g-C_3N_4 and C/g-C_3N_4(PABA:0.1%)

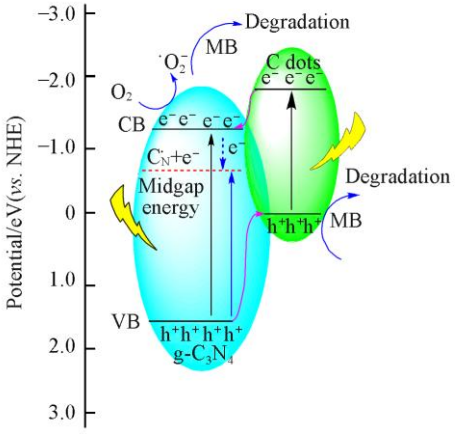

Scheme 2 Schematic diagram of MB degradation mechanism for the C/g-C_3N_4 photocatalyst

electrons in the CB of carbon dot can be readily transferred to the CB of g-C_3N_4 or captured by the midgap energy state of $C_N\cdot$ substitutional distortion/defect. Contrarily, the photo-generated holes in the VB of g-C_3N_4 can be migrated to the VB of carbon dot. The spatial separation of charge carries will inhibit the electron-hole recombination in highly efficient and thereby enhance the MB degradation over superoxide anion radicals($\cdot O_2^-$) and holes on the VB of carbon dots .

4 Conclusions

In summary, a novel *in-situ* method was established to modify g-C_3N_4 with C from urea/PABA co-crystals, with the urea serving as precursors for g-C_3N_4 and the co-former PABA acting as carbon sources. Beneficial from the advanced light absorption, the separation of charge carriers and the improved electrical conductivity, the carbon modified g-C_3N_4 could display much enhanced visible light photocatalytic activity towards MB degradation. This work demonstrates that carbon self-doping can be realized through a novel co-crystals strategy, paving a new route to design and synthesize advanced g-C_3N_4 photocatalyst through tuning the electronic band structure and textural properties of the g-C_3N_4 material.

Electronic Supplementary Material

Supplementary material is available in the online version of this article at http://dx.doi.org/10.1007/s40242-020-0073-7.

References

[1] Wang X. C., Maeda K., Thomas A., Takanabe K., Xin G., Carlsson J. M., Domen K., Antonietti M., *Nat. Mater.*, **2009**, *8*, 76
[2] Ong W. J., Tan L. L., Ng Y. H., Yong S. T., Chai S. P., *Chem. Rev.*, **2016**, *116*(12), 7159
[3] He K., Xie J., Luo X., Wen J. Q., Ma S., Li X., Fang Y. P., Zhang X. C., *Chinese J. Catal.*, **2017**, *38*(2), 240
[4] Jiang J., Cao S., Hu C., Chen C. H., *Chinese J. Catal.*, **2017**, *38*(12), 1981
[5] Liu B., Ye L., Wang R., Yang, J. F., Zhang Y. X., Guan R., Tian L. H., Chen X. B., *ACS Appl. Mater. Inter.*, **2018**, *10*(4), 4001
[6] Chen F., Yang H., Luo W., Wang P., Yu H. G., *Chinese J. Catal.*, **2017**, *38*(12), 1990
[7] Pawar R. C., Khare V., Lee C. S., *Dalton Trans.*, **2014**, *43*, 12514
[8] Yu H., Chen F., Wang X., *Appl. Surf. Sci.*, **2015**, *358*, 385
[9] Hua E. B., Liu G., Zhang G., Xu X., *Dalton Trans.*, **2018**, *47*, 4360
[10] Teng Z. Y., Yang N. L., Lv H. Y., Wang S. C., Hu M. Z., Wang C. Y., Wang D., Wang G. X., *Chem.*, **2019**, *5*, 664
[11] Jun Y. S., Lee E. Z., Wang X., Hong W. H., Stucky G. D., Thomas A., *Adv. Fun. Mater.*, **2013**, *23*(29), 3661
[12] Cui Y., Wang Y., Wang H., Cao F., Chen F. Y., *Chinese J. Catal.*, **2016**, *37*(11), 1899
[13] Zheng Y., Lin L., Ye X., Guo F., Wang X., *Angew. Chem., Int. Ed.*, **2014**, *53*, 11926
[14] Yuan B., Wei J. X., Hu T. J., Yao H. B., Jiang Z. H., Fang Z. W., Chu Z. Y., *Chinese J. Catal.*, **2015**, *36*(7), 1009
[15] Han Q., Chen N., Zhang J., Qu L. T., *Mater. Horiz.*, **2017**, *4*(5), 832
[16] Lai S. K., Xie C., Teng K. S., Li Y. Y. Tan F. R., Yan F., Lau S. P., *Adv. Opt. Mater.*, **2016**, *4*, 555
[17] Li H. L., Li F. P., Wan Z. Y., Jiao Y. C., Liu Y. Y., Wang P., Zhang X.

Y., Qin X. Y., Dai Y., Huan B., *Appl. Catal. B: Environ*., **2018**, *229*, 114

[18] Panneri S., Gangulya P., Mohan M., Naircd B. N., Mohamed A. A. P., Warrier K. G., Hareesh U. S., *ACS Sustainable Chem. Eng*., **2017**, *5*(2), 1610

[19] Vangala V. R., Chow P. S., Tan R. B. H., *Cryst. Growth Des*., **2012**, *12*(12), 5925

[20] Jun Y. S., Park J., Lee S. U., Thomas A., Hong W. H., Stucky G. D., *Angew. Chem. Int. Edit*., **2013**, *52*(42), 11289

[21] Shalom M., Guttentag M., Fettkenhauer C., Inal S., Neher D., Llobet A., Antonietti M., *Chem. Mater.*, **2014**, *26*, 5812

[22] Ishida Y., Chabanne L., Antonietti M., Shalom M., *Langmuir*, **2014**, *30*, 447

[23] Miao P., Cheng K. Y., Li H. Q., Gu J. W., Wang S., Wang D., Liu T. X., Xu B. B., Kong J., *ACS Appl. Mater. Interfaces*, **2019**, *11*(19), 17706

[24] Xu Q. L., Cheng B., Yu J. G., Liu G., *Carbon*, **2017**, *118*, 241

[25] Zhang X. F., Chen L. X., Yun J., Wang X. D., Kong J., *J. Mater. Chem. A*, **2017**, *5*(22), 10986

[26] Liu J. H., Zhang T. K., Wang Z. C., Dawsona G., Chen W., *J. Mater. Chem.*, **2011**, *21*(38), 14398

[27] Fang S., Xia Y., Lv K., LI Q., Sun J., Li M., *Appl. Catal. B: Environ*., **2016**, *185*, 225

[28] Mohamed M. A., Jaafar J., Zain M. F. M., Minggu L. J., Kassim M. B., Rosmi M. S., Alias N. H., Nor N. A. M., Salleh W. N. W., Othman M. H. D., *Appl. Surf. Sci*., **2018**, *436*, 302

[29] Shan Q. Y., Guan B., Zhu S. J., Zhang H. J., Zhang Y. X., *RSC Advances*, **2016**, *6*, 83209

[30] Wang X. F., Cheng J. J., Yu H. G., Yu J. G., *Dalton Trans*., **2017**, *46*(19), 6417

[31] Li X., Pan K., Qu Y., Wang G. F., *Nano Res*., **2018**, *11*(3), 1322

[32] Zhao Q. L., Zhang Z. L., Huang B. H., Peng J., Zhang M., Pang D. W., *Chem. Commun*., **2008**, *41*, 5116

[33] Ming H., Ma Z., Liu Y., Pan K. M., Yu H., Wang F., Kang Z. H., *Dalton Trans*., **2012**, *41*(19), 9256

[34] Bu T. J., Ma X. W., Zhao B., Song W., *Chem. Res. Chinese Universities*, **2018**, *34*(2), 290

[35] Xing W. N., Li C. M., Chen G., Han Z. H., Zhou Y. S., Hu Y. D., Meng Q., *Appl. Catal. B: Environ.*, **2017**, *203*, 65

[36] Xu Q. L., Cheng B., Yu J. G., Liu G., *Carbon*, **2017**, *118*, 241

[37] Zhao Z. W., Sun Y. J., Dong F., Zhang Y. X., Zhao H., *RSC Adv*., **2015**, *5*(49), 39549

[38] Ye C., Li J. X., Li Z. J., Li X. B., Fan X. B., Zhang L. P., Chen B., Tung C. H., Wu L. Z., *ACS Catal*., **2015**, *5*(11), 6973

[39] Kang Y. Y., Yang Y. Q., Yin L. C., Kang X. D., Liu G., Cheng H. M., *Adv. Mater.*, **2015**, *27*(31), 4572

[40] Silva E. S. D., Moura N. M. M., Coutinho A., Goran D., Faria J. L., *ChemSusChem*, **2018**, *11*(16), 2681

[41] Dong G. H., Zhao K., Zhang L. Z., *Chem. Commun*., **2012**, *48*(49), 6178

[42] She X. J., Liu L., Ji H. Y., Mo Z., Li Y. P., Huang L. Y., Du D. L., Hui X., Li H. M., *Appl. Catal. B: Environ.*, **2016**, *187*, 144

[43] Fan D., Wang Z. Y., Sun Y. J., Ho W., Zhang H. D., *J. Colloid Interface Sci*., **2013**, *401*, 70

[44] Jia Y., Chen J., Yao X. D., *Mater. Chem. Front*., **2018**, *2*, 1250

[45] Li Y. P., Wu S. L., Huang L. Y., Wang J. L., Xu H., Li H. M., *Mater. Lett.*, **2014**, *137*, 281

[46] Ding J., Wang L., Liu Q., Chai Y., Liu X., Dai W. L., *Appl. Catal. B: Environ*., **2015**, *176*, 91

[47] Cui Y. J., Ding Z. X., Liu P., Antonietti M., Fu X. Z., Wang X. C., *Phys. Chem. Chem. Phys*., **2012**, *14*, 1455

[48] Gao G. P., Jiao Y., Ma F. X., Jiao Y. L., Waclawika E., Du A. J., *Phys. Chem. Chem. Phys*., **2015**, *17*, 31140